Soft Matter

www.rsc.org/softmatter

Volume 8 | Number 14 | 14 April 2012 | Pages 3707–3996

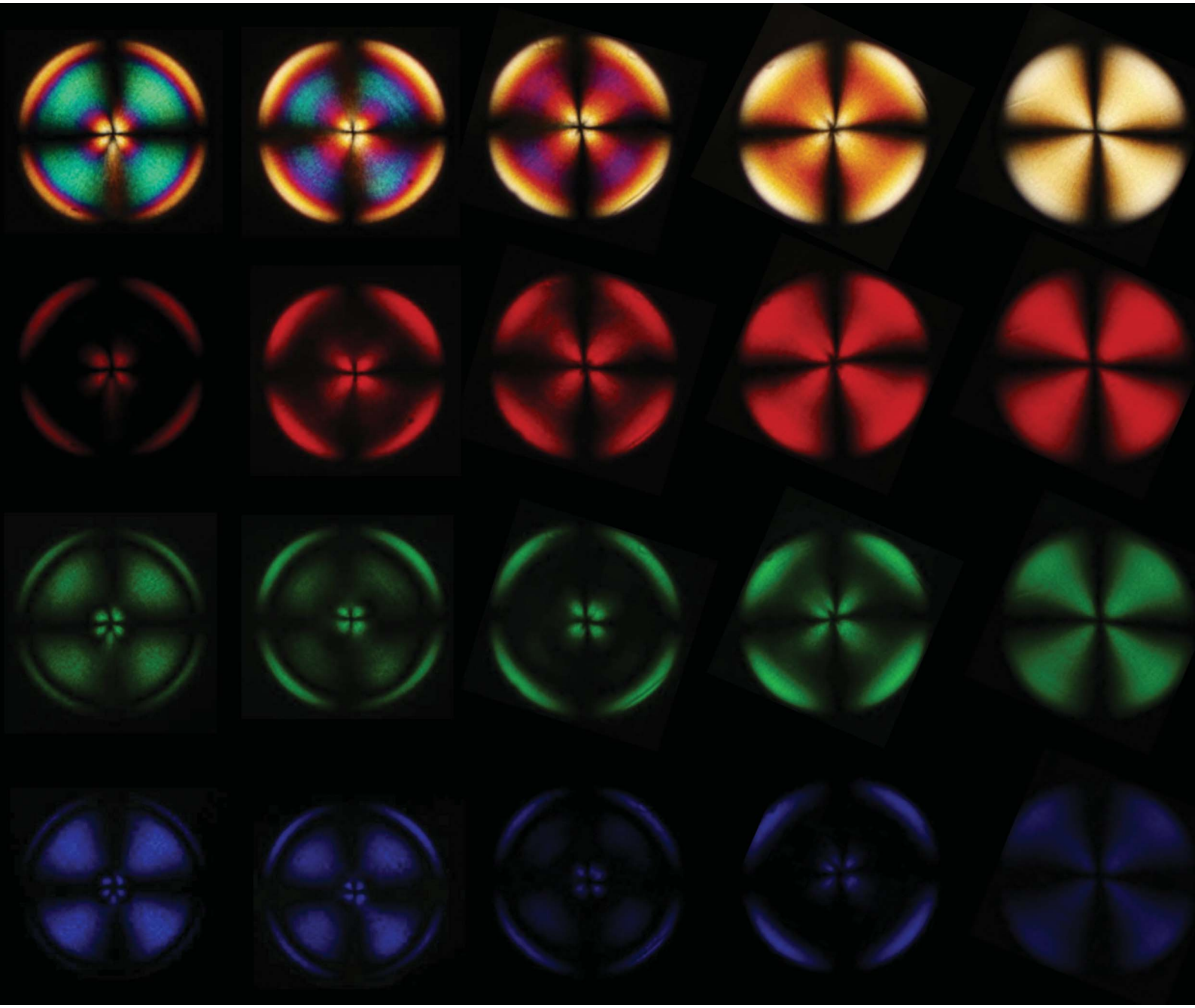

ISSN 1744-683X

RSC Publishing

PAPER

J. S. Sharp *et al.*

Giant amyloid spherulites reveal their true colours

1744-683X(2012)8:14;1-D

Soft Matter

Dynamic Article Links

Cite this: *Soft Matter*, 2012, **8**, 3751

www.rsc.org/softmatter

PAPER

Giant amyloid spherulites reveal their true colours†‡§

M. I. Smith,[a] J. S. Sharp*[ab] and C. J. Roberts[bc]

Received 19th January 2012, Accepted 30th January 2012
DOI: 10.1039/c2sm25147g

The prevalence of degenerative conditions such as Alzheimer's and Parkinson's disease amongst an increasingly elderly population has led to substantial research efforts into understanding the properties and structures of amyloid protein aggregates. One such aggregate, the amyloid spherulite, consists of a central core surrounded by long fibres of aggregated protein (fibrils) which grow radially outwards. Spherulites (5–50 μm in diameter) exhibit four white lobes when observed using crossed polarised microscopy, due to their birefringence. Here we report the growth of giant amyloid spherulites (GAS, diameters 0.4–1 mm) that produce colourful patterns when placed between crossed polarisers. A ray tracing model was developed that accounts for these patterns by calculating the effects of birefringence on light passing through the GAS. This new model links for the first time the optical properties of spherulites to the density and orientation of the fibrils, providing a route to understanding the formation of these important protein aggregates.

Introduction

Amyloid protein aggregates have been linked with a variety of important pathological conditions.[1] The most commonly studied of these aggregates are amyloid fibrils. These fibrils consist of aggregated peptide/protein molecules that pack along the fibre's axis with a cross β-sheet structure[2] (Fig. 1a). However, the potential importance of other amyloid aggregates, such as spherulites,[3] has recently been emphasised with the discovery that the peptide amyloid-β can form spherulites *in vivo*.[4]

Amyloid fibrils have two different refractive indices, depending on whether the polarisation of an incoming ray of light is parallel or perpendicular to the fibril axis (Fig. 1b).

The radial orientation of these fibrils within a spherulite causes incident rays with different polarisations to refract by different amounts and follow slightly different paths through the spherulite. For the giant amyloid spherulite (GAS) structures studied here, the path differences between these light rays are much larger than for smaller spherulites. The interference of different rays, exiting a GAS, results in the formation of coloured patterns (Fig. 2a). These patterns are similar to those observed in nematic liquid crystal drops[5,6] and treated eye lenses[7] where radially birefringent structures also exist.

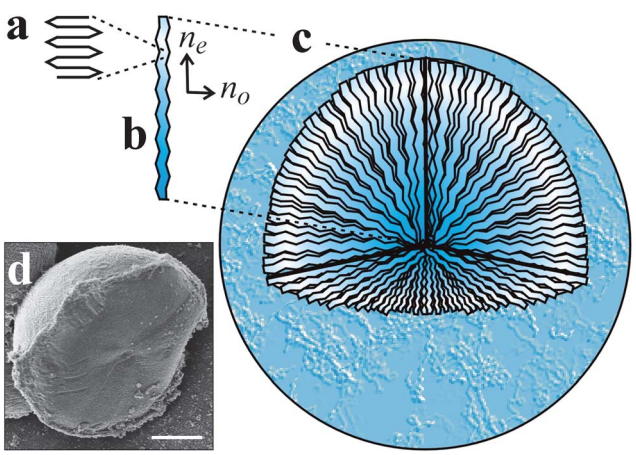

Fig. 1 Internal structure of giant amyloid spherulites (GAS). (a) Insulin molecules in a chain folded inter-molecular β-sheet structure. (b) Fibrils consist of many aggregated proteins in long thin fibres. Each fibril has an ordinary refractive index for rays polarised perpendicular to its axis and an extraordinary refractive index for those polarised parallel. (c) A schematic illustrating an idealised arrangement of fibrils inside a GAS. Fibrils are oriented radially. (d) Cryo-SEM image of the inside of a GAS. No significant core is visible suggesting that most if not all of the spherulite is composed of fibrillar material. The scale bar is 100 μm.

[a]*School of Physics & Astronomy, The University of Nottingham, Nottingham, NG7 2RD, United Kingdom. E-mail: james.sharp@nottingham.ac.uk; Tel: + 44 115 951 5142*

[b]*Nottingham Nanotechnology and Nanoscience Centre, The University of Nottingham, Nottingham, NG7 2RD, United Kingdom*

[c]*Laboratory of Biophysics and Surface Analysis, School of Pharmacy, The University of Nottingham, Nottingham, NG7 2RD, United Kingdom*

† Electronic supplementary information (ESI) available. See DOI: 10.1039/c2sm25147g

‡ Author Contributions: MIS performed the experiments, produced the model and performed the analysis. MIS, JSS and CJR designed the experiments and wrote the paper.

§ Author Information: The authors declare no competing financial interests. Correspondence and requests for materials should be addressed to james.sharp@nottingham.ac.uk

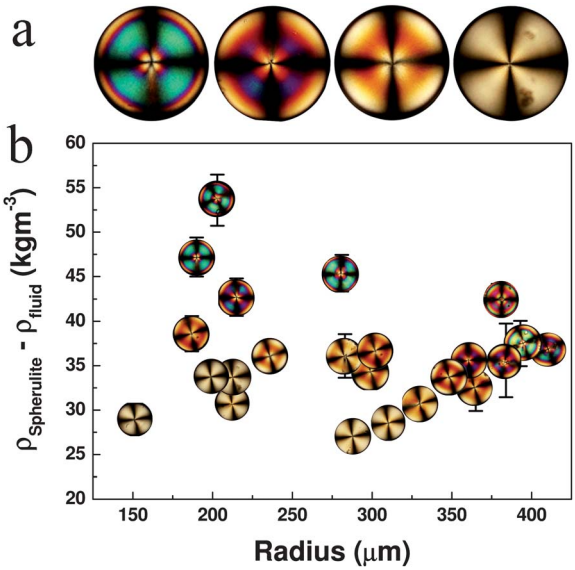

Fig. 2 Relating optical and structural properties of spherulites. (a) Example of GAS showing the range of colourful patterns (isochromes) that are observed. (b) Mean density measurements of individual spherulites obtained from sedimentation kinetics. More colourful patterns are observed as the spherulite density and radius increase. The average reduced density ($\rho_{spherulite} - \rho_{liquid}$) of conventional spherulites has been reported to be 34.5 kg m^{-3} which is in good agreement with the lower end of our measured range.[5]

Materials and methods

GAS structures were formed from Bovine Insulin (10 mg ml^{-1}, pH 2.8, 25 mM NaCl) by incubation in sealed glass vials ($T = 67$ °C). After 24 h a 2 ml sample was typically found to contain just 30–50 spherulites (Diameter ~400–1000 μm). GAS stained with the amyloid dye Thioflavin-T were found to fluoresce brightly, indicating that they contain amyloid species (*e.g.* fibrils).

Results

GAS with similar radii taken from the same vial were found to display different patterns when viewed through crossed polarisers (Fig. 2a). Some exhibited brightly coloured rings (isochromes), while others displayed uniform white lobes. This indicates that differences exist in the internal structure of GAS formed under similar conditions. Conventional spherulites often contain a central core composed of disordered protein aggregates.[3] The presence of a core would affect the optical properties of a spherulite, altering the refraction and birefringence of the central region. However, Cryo-SEM of GAS revealed no evidence of a sizeable core (Fig. 1d). This suggests that other structural differences in *e.g.* packing density and/or orientation of fibrils, may exist between GAS aggregates.

The densities, ρ, of individual GAS of radius, R, were used to determine the effect of such structural differences on the isochromes. Individual GAS were deposited at the top of a measuring cylinder containing deionised water. Their density was then calculated from measurements of their terminal sedimentation velocity (V) using:

$$\rho_{Spherulite} - \rho_{Liquid} = \frac{9V\eta}{2gR^2} \quad (1)$$

where η is the viscosity of water and g is the acceleration due to gravity.[8] Fig. 2b shows the density of GAS as a function of their radius. A clear correlation is observed between the density and/or radius of the GAS aggregates and the isochromes produced. An increased density indicates a higher packing fraction of fibril within the spherulite. Consequently, as the radius and/or density increases, incoming rays will pass through more fibrillar material whilst traversing the spherulite. This increases the path difference between rays polarised parallel and perpendicular to the fibril axis. When these path differences become comparable to the wavelength of light, constructive and destructive interference gives rise to coloured fringes (Figs. 2 and 3).

The refractive index of the liquid surrounding the spherulite, also influences the isochromes. Images of GAS in water–glycerol mixtures (n_{liq} = 1.333 – 1.473) under crossed polarisers were collected using a x10 microscope objective (Fig. 3). In the highest refractive index mixtures (where the index difference of fibril and fluid is small) all spherulites appeared white. However, when the refractive index difference was increased (low index fluid), isochromes were formed.

Adjusting the refractive index of the liquid surrounding the GAS alters the amount of refraction at the surface of the spherulite. This changes the angle of propagation and introduces small differences in the pathlength of each ray. However, this effect is minor and unable to account for the observed changes in the isochromes. Changing the suspending solvent also affects the birefringence of the GAS. This birefringence has two components, the first of which is the *intrinsic* birefringence of the fibrils. This arises as a result of the different polarisabilities parallel and perpendicular to their axes (Fig. 1a). Secondly, shielding of the polarisation charges in the fibrils by a surrounding dielectric liquid will be anisotropic (*i.e.* different parallel and perpendicular to fibril axis). This gives rise to a so called *form* birefringence which depends upon the refractive index of the suspending liquid.[9]

The model

A Matlab (Mathworks) based ray tracing model was developed in order to predict the positions of the isochromes observed in the optical micrographs. The GAS model considers 2000 rays travelling through a 2D disc which passes through the centre of the structure (Fig. 4) and which is composed of 1000 segments (supplementary information† 1 & 2). Each segment has an ordinary (perpendicular) and extraordinary (parallel) refractive index (Fig. 4) similar to a fibril (or a bundle of fibrils). The component of the ray polarised perpendicular to the disc, refracts only at the outer surfaces of the GAS as this component just experiences the ordinary refractive index. However, the component of the ray polarised in the plane of the disc encounters a varying refractive index as it passes through the structure and is refracted at each segment boundary due to the changing fibril orientation (supplementary information† Fig. 2).[10] The effects of refraction on rays leaving the GAS are then also calculated. Having modelled the ray path through the spherulite disc we

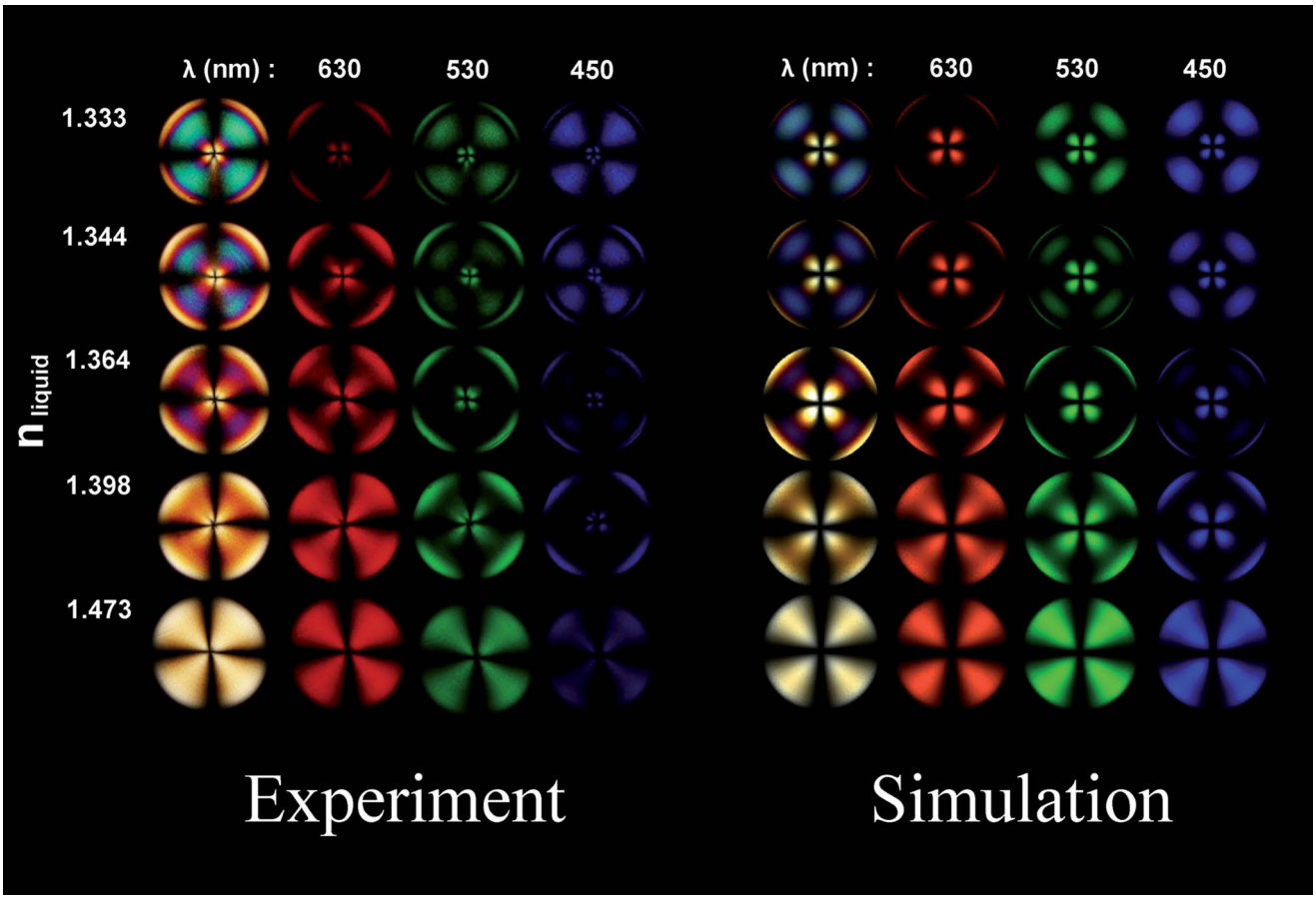

Fig. 3 Experimental and simulated images of a single GAS. The GAS (radius 190 μm, mean density 1.047 kg m^{-3}) was immersed in water–glycerol mixtures with different refractive indices. The left hand set of images show all the isochromes that are observed when the GAS is placed between crossed polarisers and illuminated with white light. The next three columns show individual isochromes that are observed by placing single colour filters in front of the light source. The images on the right hand side show the results of simulations obtained using the ray tracing model described in the text.

produce the full 3D spherulite by rotating the disc around the vertical axis in Fig. 4.

The image formed at the CCD camera is the same as the virtual image formed at S in Fig. 4, where the rays *appear* to originate. Mapping individual rays to individual pixels on a screen (at S) enables us to build up an image of the spherulite. The effects of polarisers on the transmitted intensity of each ray are calculated by resolving the polarisation of the output rays in the direction of the polariser axes. Finally, the path difference between rays which appear to have come from the same position in the virtual image is calculated (ESI,† Fig. S3). We note that a result of this is that interfering ordinary and extraordinary rays often originate from different points on the initial wavefront.

Our model was used to estimate the mean refractive index and birefringence of the spherulite when immersed in liquids of different refractive index (supplementary information† 4). Assuming refractive index values for insulin ($n_p = 1.544$[11]) and the water-glycerol mixtures[12] (n_{liq}) we estimate the volume fraction of protein ($\varphi = 0.36$) in the spherulites by fitting their fluid dependent refractive index values obtained from experiment (Fig. 4b).[9]

$$n \approx (n_{liq}^2(1 - \phi) + n_p^2\phi)^{0.5} \quad (2)$$

This value was then used to calculate the magnitude of the form birefringence (dn_{form}) assuming that fibrils are infinitely long rods.[9]

$$dn_{form} = n\left(1 - \left(\frac{1 + \left(\frac{n_p}{n}\right)^2}{2\left(1 - \frac{(n^2 - n_p^2)}{2n_{liq}^2}\right)}\right)^{0.5}\right) \quad (3)$$

Finally, using fits of eqn (4) to values of the total birefringence obtained from fits of our model to images of spherulites (ESI,† Fig. S4) we calculate the intrinsic birefringence, and an order parameter (S), which characterises how well the fibrils are aligned radially.

$$dn = S(dn_{intrinsic} + dn_{form}(\phi, n_{liq})) \quad (4)$$

The fits shown in Figs. 4b & c give an intrinsic birefringence of 0.004 and a form birefringence in water of 0.009. Our results suggest a fairly small value for the order parameter ($S = 0.27$). This could be interpreted as poor ordering, or alternatively as an indication of large amounts of branching of the fibrils that comprise the spherulite.

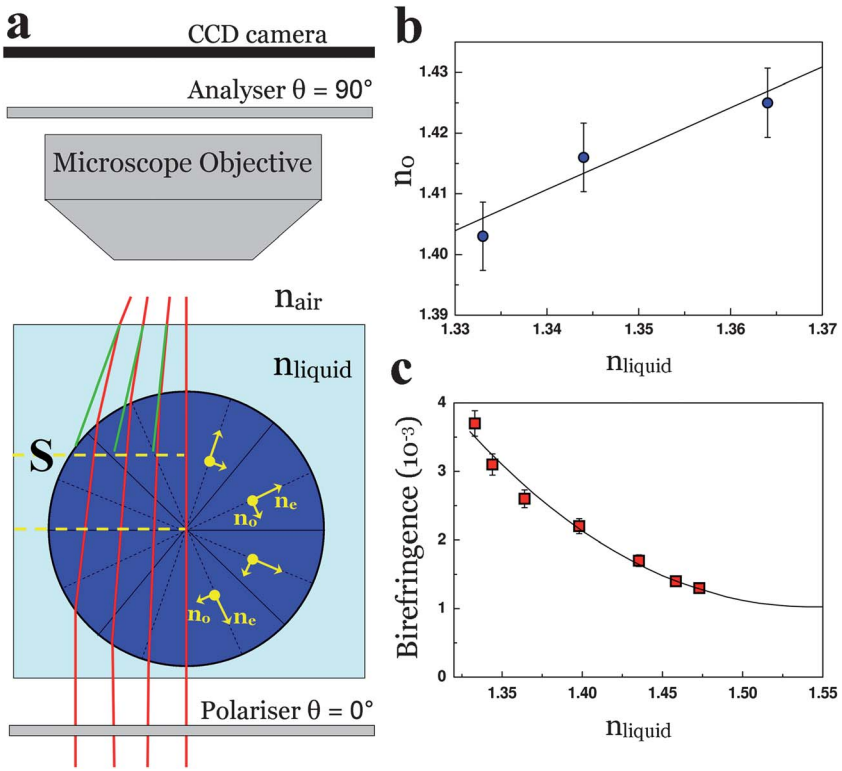

Fig. 4 The spherulite model. (a) The spherulite is treated as a 2-D disc with 1000 segments. Each segment has a birefringence such that the axis of the fibrils/fibril bundles is/are radial. Rays enter the disc and are split into two polarisations; parallel (extraordinary) and perpendicular (ordinary) to the plane of the disc. A virtual image is formed at S. Rotating the 2-D disc about its vertical axis results in the formation of a full 3-D model. Finally, the effect of polarisers, the objective and interference are then calculated for each ray. (b & c) The model is used to make estimates of the mean refractive index and birefringence of a spherulite in different refractive index liquids. Fits of eqn (2) & (4) enable us to calculate the intrinsic and form birefringence as well as the orientational parameter (S).

Discussion and conclusions

Fig. 3 shows a comparison of our model with experimental images for a single spherulite.We see good agreement, which indicates that our model captures the essential physics. The symmetry of the isochromes with increasing radius can be explained by considering how the optical path, Δ(nd), changes for rays that are incident at different positions. Near the centre, the distance travelled (d) is a maximum, but the two polarisations experience the same refractive index (n_o) since they travel down a fibril axis. At the edge of the disc, different polarisations experience the maximum difference in refractive index (n_e–n_o), but the distance travelled by the rays inside the spherulite is small. In both the above cases Δ(nd) will be small. At some intermediate radial position, Δ(nd) becomes large and there is a maximum in the path difference (Fig. 2a).

Some differences exist between the simulations and experiments. In particular the central lobes observed in the simulations extend to larger radii than those observed in experiment. The edges of the coloured features in the simulations also extend further outwards in a radial direction than in the microscope images. This suggests that the path difference is being underestimated near the spherulite centre and overestimated at the periphery. This is probably caused by the assumption that the density is uniform throughout the GAS. In reality this would be surprising, since variations in the local packing and branching of fibrils are likely to occur with increasing radius. It is also possible that the order parameter changes with radius and the local fibril packing density. Whilst the order parameter and spherulite volume fraction are expected to vary within and between spherulites, one would expect the intrinsic birefringence, which is just a property of individual fibrils to be a general property of all GAS.

An additional factor, not considered in this study, is that amyloid spherulites may contain a proportion of amorphous protein in amongst the packed fibrils as is observed in polymer spherulites. This fraction is likely to be sensitive to the kinetics of the assembly process and will depend upon experimental conditions such as temperature. We would expect the amorphous fraction to contribute to the index of refraction of the GAS structures. As a result of this our estimates of the volume fraction of birefringent material are likely to be slightly higher than the true values. This would lead to a small error in the calculated form birefringence but would not affect the calculated intrinsic birefringence or the order parameter.

We have shown that the isochromatic patterns that are generated when GAS are viewed between crossed polarisers can be explained and modelled in terms of the birefringent properties of the fibrils that comprise these structures. This model has the potential to provide detailed information about the internal packing and orientational order of fibrils within the GAS. This will provide insights into the processes that result in the

formation of potentially harmful protein aggregates and strategies for the development of diagnostics and therapeutics.

Acknowledgements

We acknowledge the financial support of the EPSRC, UK (grant ref. EP/H004939/1). We also thank Dr. Chris Parmenter for collecting the cryo-SEM images.

References

1 C. M. Dobson, *Science*, 2004, **304**, 1259–1262.
2 C. M. Dobson, *Nature*, 2002, **418**, 729–730.
3 M. R. H. Krebs, C. E. MacPhee, A. F. Miller, I. E. Dunlop and C. M. Dobson, *Proc. Natl. Acad. Sci. U. S. A.*, 2004, **101**, 14420–14424.
4 C. Exley, E. House, J. F. Collingwood, M. R. Davidson, D. Cannon and A. M. Donald, *J. Alzh. Dis.*, 2010, **20**, 1159–1165.
5 A. Fernández-Nieves, D. R. Link, M. Márquez and D. A. Weitz, *Phys. Rev. Lett.*, 2007, **98**, 087801.
6 R. Ondris-Crawford, E. P. Boyko, B. G. Wagner, J. H. Erdmann, S. Žumer and J. W. Doane, *J. Appl. Phys.*, 1991, **69**, 6380–6386.
7 B. K. Pierscionek, *Exp. Eye Res.*, 1994, **59**, 121–124.
8 T. E. Faber, *Fluid dynamics for physicists*, Cambridge University Press, Cambridge, UK, 1995.
9 R. C. Haskell, F. D. Carlson and P. S. Blank, *Biophys. J.*, 1989, **56**, 401–413.
10 W. D. Nesse, *Optical mineralogy* 3rd Edition, Oxford University Press, Oxford, UK, 2004.
11 A. Maschke, N. Calí, B. Appel, J. Kiermaier, T. Blunk and A. Göpferich, *Pharm. Res.*, 2006, **23**, 2220–2229.
12 L. F. Hoyt, *Ind. Eng. Chem.*, 1934, **26**, 329–332.